Study of the spatial characteristics of emission of surface-emitting ring quantum-cascade lasers

© A.V. Babichev[1], D.A. Mikhailov[2], D.V. Chistyakov[2], E.S. Kolodeznyi[1], A.G. Gladyshev[1], G.V. Voznyuk[2], M.I. Mitrofanov[2,4], D.V. Denisov[3], S.O. Slipchenko[2], A.V. Lyutetskii[2], V.V. Dudelev[2], V.P. Evtikhiev[2], L.Ya. Karachinsky[1], I.I. Novikov[1], N.A. Pikhtin[2], A.Yu. Egorov[5], G.S. Sokolovskii[2]

[1] ITMO University,
197101 St. Petersburg, Russia
[2] Ioffe Institute,
194021 St. Petersburg, Russia
[3] St. Petersburg State Electrotechnical University „LETI"
197022 St. Petersburg, Russia
[4] Submicron Heterostructures for Microelectronics, Research and Engineering Center, Russian Academy of Sciences,
194021 St. Petersburg, Russia
[5] Alferov Federal State Budgetary Institution of Higher Education
and Science Saint Petersburg National Research Academic University of the Russian Academy of Sciences,
194021 St. Petersburg, Russia

E-mail: a.babichev@mail.ioffe.ru

Received March 1, 2022
Revised March 24, 2022
Accepted March 24, 2022

The results of studies of ring quantum-cascade lasers with surface emission due to a second-order grating formed in the top cladding layers are presented. Surface emission near 7.85 μm with a low threshold current density (3.8 kA/cm^2), in comparison with ridge quantum-cascade lasers of the same cavity length is demonstrated. The results of measurements of the intensity distribution of the near and far fields at different pumping levels are presented. The estimated value of the angle of beam extraction relative to the surface normal is in the range $(5.7-6.7)^\circ$.

Keywords: ring cavity, grating, focused ion beam (FIB) etching, superlattices, quantum-cascade laser, epitaxy, indium phosphide.

DOI: 10.21883/SC.2022.06.53547.9825

1. Introduction

Quantum-cascade lasers (QCL) of the $8-12\,\mu$m spectral range are of interest for the making of chemical element recognition systems (chemical fingerprinting) [1,2], including due to the possibility of integration on one chip [3,4]. Due to the TM polarization of radiation observed in intersubband transition lasers [5], surface out-coupling can be implemented by formation of a one-dimensional [6,7] or two-dimensional diffraction grating (based on photonic crystals [8,9]). At the same time, implementation of lasing in a continuous regime of current pumping in the design of photonic crystals is difficult. In its turn, the use of a design of a ring cavity and a diffraction grating of the 2-nd order on the entire cavity surface makes it possible to implement lasing in the continuous current pumping regime at room temperature with the output optical power of ~ 0.2 W [10,11].

A diffraction grating in a QCL with a ring cavity is used both for selection of optical modes and for surface out-coupling. Moreover, the ring cavity design can be used for selection of azimuthal modes [12–15], and a distributed Bragg reflector (DBR) — for surface out-coupling.

DBR sections are traditionally used for selection of optical modes in stripe lasers [16–18], while the use of additional DBR sections excludes the effect of an uncontrolled phase „incursion" upon stripe laser shearing [19]. Formation of a diffraction grating of the 2-nd order between two DBR sections allows for surface out-coupling [20,21]. The results concerning the influence of a diffraction grating of the 2-nd order on the parameters of surface out-coupling in stripe lasers are given in [7]. However, the results for a QCL in a ring design were not considered.

This paper presents the results of study of the near and far field of a QCL with a ring cavity with out-coupling through a diffraction grating of the 2-nd order formed on the ring cavity surface by direct ion lithography with a focused ion beam.

2. Experimental samples

A QCL heterostructure was grown by molecular-beam epitaxy [22]. A buffer layer of $In_{0.53}Ga_{0.47}As$ 500 nm thick was formed on an InP substrate with the crystallographic orientation $(100) \pm 0.5^\circ$. The cascade layers were formed based on the $In_{0.53}Ga_{0.47}As/Al_{0.48}In_{0.52}As$ heteropair in a design with two-phonon depopulation of the lower level. The total thickness of active region layers was 2.63 μm. The waveguide upper cladding was formed based on

indium phosphide 3.9 μm thick with the doping level of $1.0 \cdot 10^{17}$ cm^{-3}. The contact layers of $In_{0.53}Ga_{0.47}As$ with a variable doping level of $1.0 \cdot 10^{17}$ cm^{-3} and $1.0 \cdot 10^{19}$ cm^{-3} had the total thickness of 120 nm. The following processing steps were used when forming ring cavity crystals: liquid etching of the mesa, deposition of dielectric, opening of a window in dielectric, deposition of upper metallization layers, substrate thinning, deposition of lower metallization layers. The mesastructure was etched with inoculation into the substrate. The ring cavity radius measured in the middle point was 191 μm. The ring cavity width near the surface was 20 μm. For measurements, the ring cavity crystal was mounted with the substrate downwards onto a copper heat sink by means of indium solder.

A diffraction grating was formed on the cavity segment in ultra-high vacuum by a focused ion beam of gallium, ion energy being 30 keV and operating current being 490 pA [23]. The ion dose during etching of diffraction grating grooves was $1.4 \cdot 10^{11}$ pK/cm^2. The diffraction grating period in angular coordinates was 0.71° (corresponds to $\Lambda \sim 2.367\,\mu$m with the ring cavity radius of 191 μm). Duty ratio was 60%. Groove etching depth was 2097 ± 100 nm (with account of thickness of the upper metallization layers) (Fig. 1). Selection of etching depth was determined during numerical calculations. It has been previously shown that the use of a strong bonding regime causes lasing at higher-order modes [10,11,24]. The estimated value of the binding coefficient κ on binding length L in the coupled-mode theory [25]) is defined as a „leap" of real and imaginary parts of the effective refraction index in etched and non-etched regions of a diffraction grating. The typical values for implementation of the single-frequency lasing regime are $\kappa \sim 16\,\text{cm}^{-1}$ ($\kappa L \sim 1.6$) [26] for the case of index coupling and $\kappa = (1.52 + 4.91i)\,\text{cm}^{-1}$ ($\kappa L = 0.4 + 1.2i$) for the case of complex coupling [11]. The estimated value of κ for the studied diffraction grating was $\sim 3.9\,\text{cm}^{-1}$. Binging region length L is 223 μm. Quantity $\text{Abs}(\kappa L) \sim 0.1$. Quantity $\text{Abs}(\kappa L)$ will be equal to ~ 0.5 when a diffraction grating is formed on the entire cavity surface.

Lasing spectra were measured using a Bruker Vertex 70v Fourier spectrometer at 294 K. The optical signal was detected using a HgCdTe photodiode. The spectral resolution was 0.16 cm^{-1}. Duration of pumping current pulses τ was 200 ns when studying radiation spectra, and $\tau = 70$ ns when studying current-voltage, current-power characteristics. Pulse repetition rate f was 25 kHz.

Spatial characteristics in the near and far field zone were recorded using a Dataray WinCamD-IR-BB bolometric camera with the resolution of 640×480 pixels (pixel size $17 \times 17\,\mu\text{m}^2$). When studying the near field, the image was projected on the camera surface by means of a lens with the focal distance of 3 mm and number aperture 0.56. The magnification coefficient was 200. When studying the far field, the image was recorded directly (without focusing lenses) with the bolometric camera at the distance of 7.5 mm. Duration of pumping pulses during measurement of spatial characteristics was 70 ns, pulse repetition rate was 48 kHz. All the measurements were performed at 291°C.

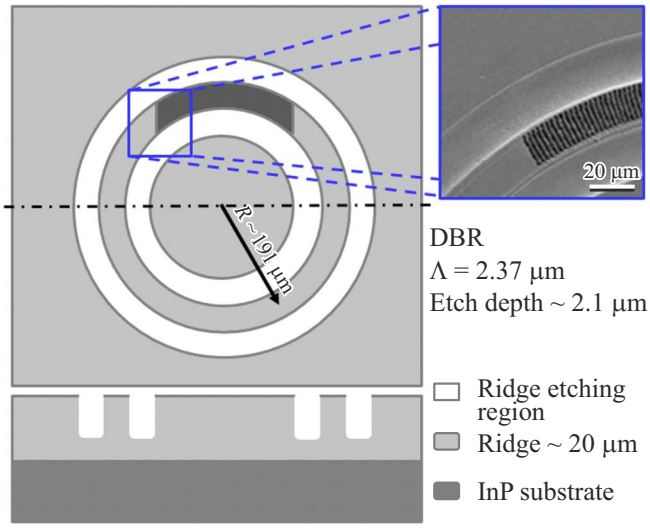

Figure 1. Schematic view of QCL with a ring cavity (top view and cross-section). The insert shows a scanning electron microscopy image of the formed diffraction grating (top view).

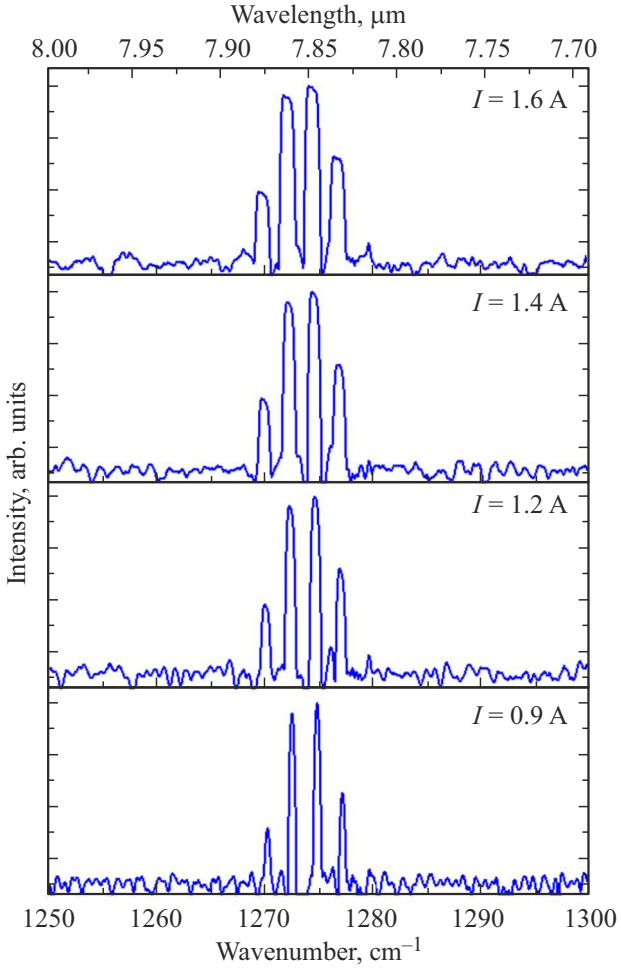

Figure 2. Spectra of surface lasing for QCL with ring cavity.

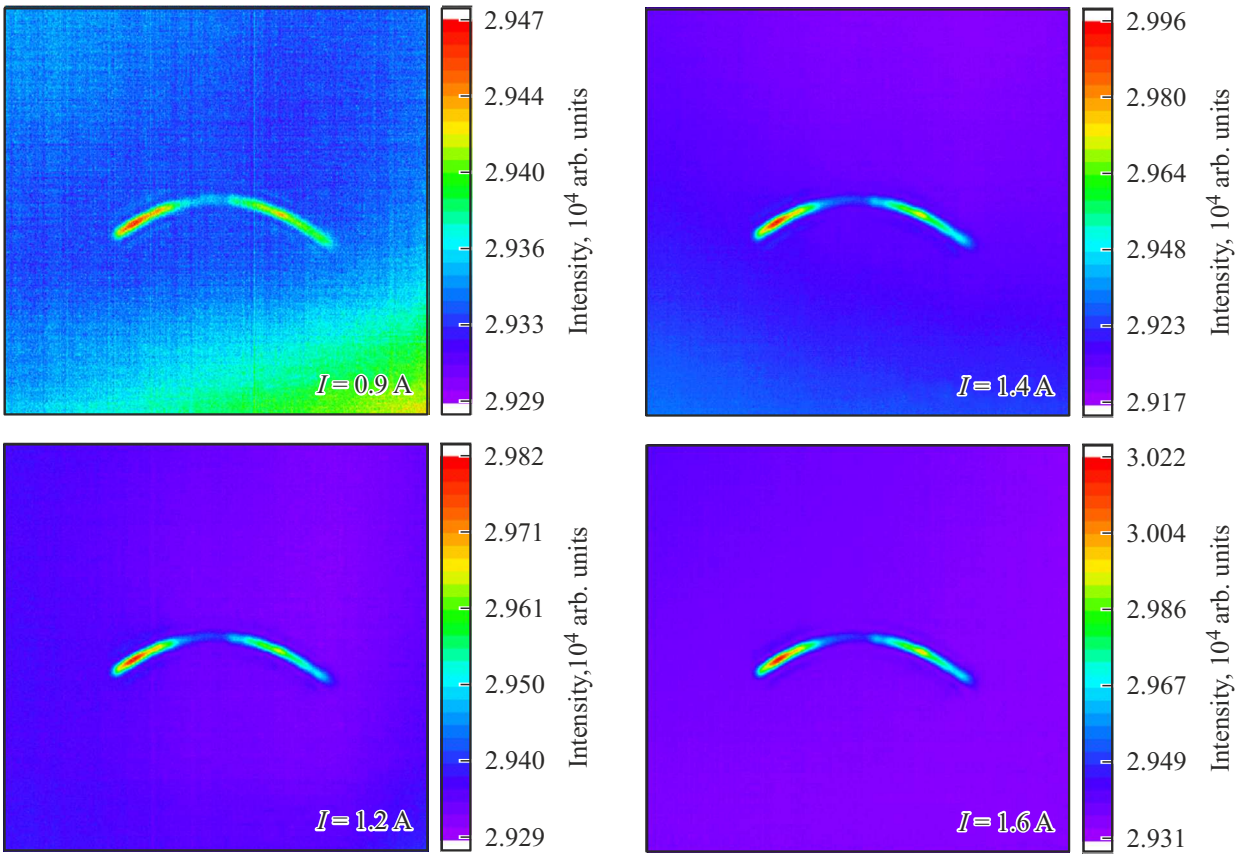

Figure 3. Distribution of radiation intensity in the near field zone. (A colored version of the figure is presented in the electronic version of the article.)

3. Results and discussion

The normalized spectra of surface lasing under different current pumping levels are shown in Fig. 2 in the semi-logarithmic scale. The lasing spectra near the threshold current value $I_{th} = 0.8$ A (threshold current density was 3.8 kA/cm^2) are represented by four lines (modes) near 7.85 μm. The intermodal distance was $\sim 2.3\,\mathrm{cm}^{-1}$, corresponding to the case of consideration of whispering gallery modes. The group reflection coefficient was estimated, its value was $n_{group} \sim 3.39$. It has been previously shown [27] that, when the value of ring cavity strip width is $\sim 4\,\mu$m, optical losses for transverse (radial) higher-order modes considerably increase; this causes single-frequency lasing. In its turn, when width of the ring cavity strip is $\sim 10\,\mu$m, the lasing spectrum may contain a second radial mode. The papers [27,28] showed the presence of a second lasing line located at 43 nm from the principal mode. The samples studied by us did not display this effect. Paper [29] showed that the spectrum contains longitudinal (azimuthal) higher-order modes when the weak binding regime is implemented ($\kappa \sim 0.1\,\mathrm{cm}^{-1}$, $\mathrm{Abs}(\kappa L) \sim 0.01$). In this respect, it can be suggested that the multimode pattern of lasing in the studied samples, where the estimated value of $\mathrm{Abs}(\kappa L)$ is higher by an order, is either due to a mismatch of the spectral position of the Bragg wavelength to the maximum of the amplification spectrum [30], or due to a relatively small value of optical losses introduced by the diffraction grating. The authors have previously demonstrated single-frequency lasing at the radiation wavelength of $\lambda = 7.778\,\mu$m for half-ring QCLs with the radius of 191 μm and a similar heterostructure design [15]. To sum up, there is a mismatch between the spectral position of the Bragg wavelength and the amplification spectrum maximum (7.778 μm).

Increase of the current pumping level causes a long-wavelength shift of the radiation wavelength. Taking into account the value of temperature shift of the radiation wavelength for the presented heterostructure design in a stripe laser ($\Delta\lambda/\Delta T = 0.56$ nm/K [31]), we estimated the laser temperature increase upon current pumping increase from 0.9 to 1.6 A, which was equal to $\sim 6^\circ$C. A detailed analysis of radiation wavelength shift with temperature should be performed in the single-frequency lasing regime [26].

The results of study of radiation intensity distribution in the near field zone are shown in Fig. 3. The dimensions (total length) of the radiation region near the lasing threshold correlate with the dimensions of the region of the ring cavity segment with a diffraction grating ($\sim 67^\circ$). At the same time, an intensity „gap“ should be noted, due to which the field is divided into two regions in the direction

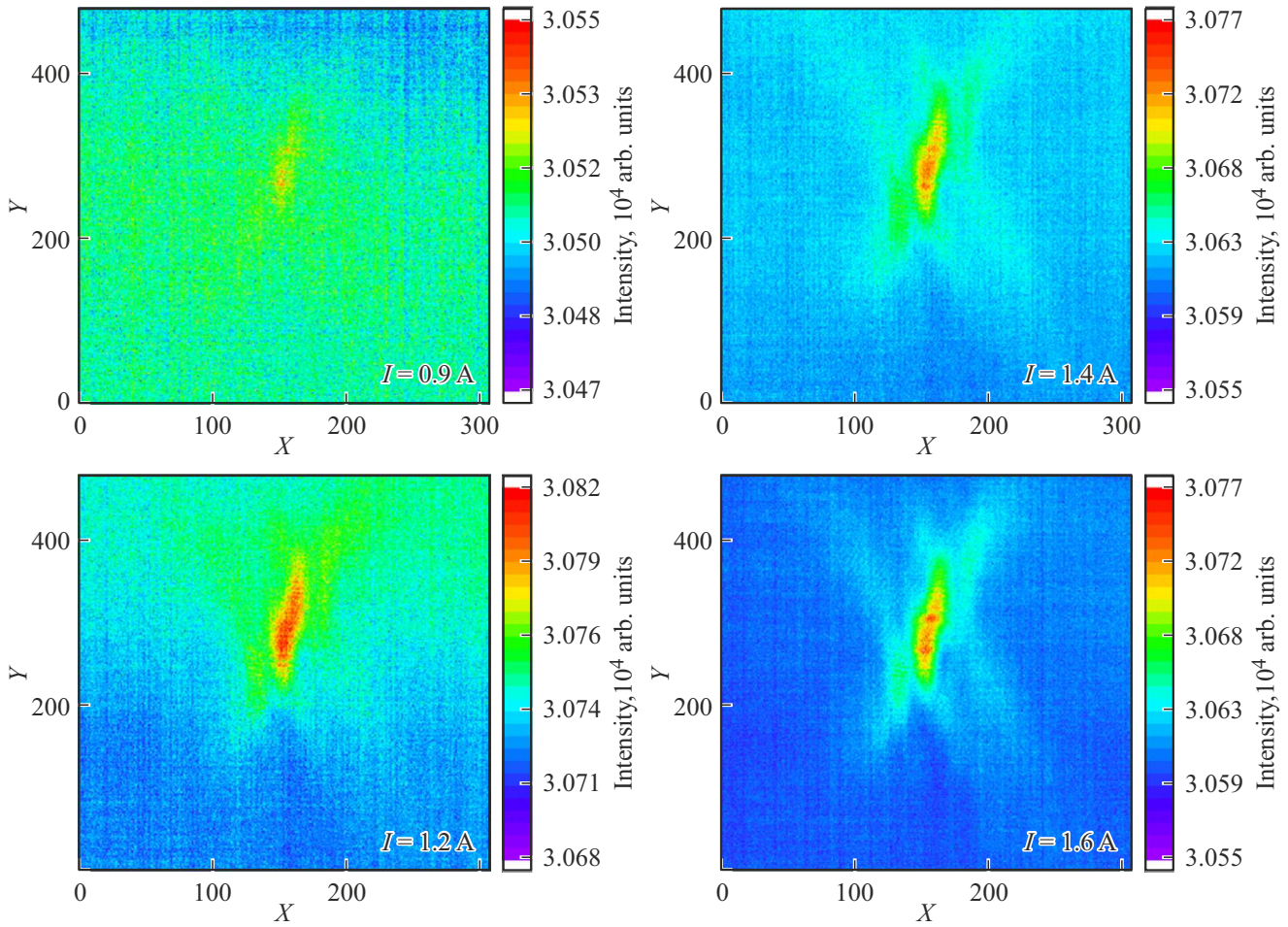

Figure 4. Distribution of radiation intensity in the near field zone. (A colored version of the figure is presented in the electronic version of the article.)

Dependence of out-coupling angle on level of laser current pumping

Level of current pumping, A	λ_0, μm/α_0, deg	λ_1, μm/α_1, deg	λ_2, μm/α_2, deg	λ_3, μm/α_3, deg
0.9	7.873/−6.55	7.858/−6.19	7.844/−5.85	7.830/−5.50
1.2	7.874/−6.58	7.860/−6.23	7.845/−5.87	7.831/−5.53
1.4	7.875/−6.60	7.861/−6.26	7.847/−5.92	7.832/−5.55
1.6	7.877/−6.71	7.863/−6.31	7.849/−5.97	7.834/−5.60

of 20 and 32° respectively. The near field for a QCL with a diffraction grating, formed on the entire cavity length, was previously represented by homogeneous radiation present along the entire ring cavity perimeter [32,33]. Pumping current increase to $2I_{\text{th}}$ did not cause a redistribution of radiation intensity and disappearance of the intensity gap, which can be due to the inhomogeneity of diffraction grating parameters because of a significant depth of the etched DBR, similarly to the results given for interband cascade lasers with a ring cavity [27].

The results of study of intensity distribution in the far field are shown in Fig. 4. It has been previously shown that multimode lasing leads to a considerable modification of intensity distribution in the far field of the ring cavity and increase in the total width, measured at half-height from 3 to 10° [34].

Out-coupling angle α in relation to the normal to the surface will be determined based on expression $\alpha = \arcsin\left(\text{Re}(n_{\text{eff}}/n_0) - \lambda/(\Delta n_0)\right)$, where n_{eff} — effective refraction index of the laser, n_{air} — effective refraction index of the second medium, air in this case, λ — lasing wavelength [7,34]. Out-coupling angle α_i was estimated based on this expression (see the table). The effective refraction index can be estimated based on the expression $n_{\text{eff}} = \lambda/\Lambda$, where λ is radiation wavelength in the single-frequency lasing regime [29]. Due to the multimode lasing

regime in the studied QCLs, an estimated value of n_{eff} was used when estimating the out-coupling angle. It has been shown that when the spectrum contains four lasing lines (azimuthal optical modes), the out-coupling angle varies within $-(5.5-6.7)^\circ$, which may cause a modification of radiation intensity in the far field shown in Fig. 4.

4. Conclusion

Surface lasing near $7.85\,\mu$m has been demonstrated. A ring cavity laser demonstrates a low density of threshold current ($3.8\,\text{kA/cm}^2$) as compared to stripe lasers of the same length. The multimode lasing pattern hinders a correct interpretation of the obtained results of intensity distribution in the far field of a ring QCL because radiation is present at several wavelengths with typical divergence angles for each wavelength. The estimated values of the out-coupling angle in relation to a normal to the surface are within $(5.7-6.7)^\circ$. In future, the use of a greater coefficient of index coupling or implementation of a complex-coupling mechanism [11] must allow for implementation of the single-frequency lasing regime in a ring QCL.

Funding

The work has been funded by a grant of the Russian Science Foundation (project No. 20-79-10285).

Conflict of interest

The authors declare that they have no conflict of interest.

References

[1] A. Harrer, R. Szedlak, B. Schwarz, H. Moser, T. Zederbauer, D. MacFarland, H. Detz, A.M. Andrews, W. Schrenk, B. Lendl, G. Strasser. Sci. Rep., **6** (1), 31236 (2016).
[2] F. Kapsalidis, M. Shahmohammadi, M.J. Süess, J.M. Wolf, E. Gini, M. Beck, M. Hundt, B. Tuzson, L. Emmenegger, J. Faist. Appl. Phys. B: Lasers Opt., **124** (6), 107 (2018).
[3] R. Szedlak, J. Hayden, P. Martín-Mateos, M. Holzbauer, A. Harrer, B. Schwarz, B. Hinkov, D. MacFarland, T. Zederbauer, H. Detz, A.M. Andrews, W. Schrenk, P. Acedo, B. Lendl, G. Strasser. Opt. Eng., **57** (1), 011005 (2017).
[4] R. Szedlak, A. Harrer, M. Holzbauer, B. Schwarz, J.P. Waclawek, D. MacFarland, T. Zederbauer, H. Detz, A.M. Andrews, W. Schrenk, B. Lendl, G. Strasser. ACS Photonics, **3** (10), 1794 (2016).
[5] O. Spitz, A. Herdt, M. Carras, W. Elsäßer, F. Grillot. In: *OSA Tech. Digest* (San Jose, CA, USA, Optica Publishing Group, 2019), paper SW3N.2. DOI: 10.1364/CLEO_SI.2019.SW3N.2
[6] C. Pflügl, M. Austerer, W. Schrenk, S. Golka, G. Strasser, R. Green, R.P. Green, L.R. Wilson, J.W. Cockburn, A.B. Krysa, J.S. Roberts. Appl. Phys. Lett., **86** (21), 211102 (2005).
[7] E. Cristobal, H. Shu, A. Lyakh. AIP Advances, **11** (11), 115221 (2021).
[8] Z. Wang, Y. Liang, B. Meng, Y.T. Sun, G. Omanakuttan, E. Gini, M. Beck, I. Sergachev, S. Lourdudoss, J. Faist, G. Scalari. Opt. Express, **27** (16), 22708 (2019).
[9] S. Saito, R. Hashimoto, K. Kaneko, T. Kakuno, Y. Yao, N. Ikeda, Y. Sugimoto, T. Mano, T. Kuroda, H. Tanimura, S. Takagi, K. Sakoda. Appl. Phys. Express, **14** (10), 102003 (2021).
[10] Y. Bai, S. Tsao, N. Bandyopadhyay, S. Slivken, Q.Y. Lu, D. Caffey, M. Pushkarsky, T. Day, M. Razeghi. Appl. Phys. Lett., **99** (26), 261104 (2011).
[11] D.H. Wu, M. Razeghi. APL Materials, **5** (3), 035505 (2017).
[12] P.Q. Liu, K. Sladek, X. Wang, J.Y. Fan, C.F. Gmachl. Appl. Phys. Lett., **99** (24), 241112 (2011).
[13] P.Q. Liu, X. Wang, J.Y. Fan, C.F. Gmachl. Appl. Phys. Lett., **98** (6), 061110 (2011).
[14] A.V. Babichev, A.G. Gladyshev, A.S. Kurochkin, V.V. Dudelev, E.S. Kolodeznyi, G.S. Sokolovskii, V.E. Bugrov, L.Ya. Karachinsky, I.I. Novikov, D.V. Denisov, A.S. Ionov, S.O. Slipchenko, A.V. Lyutetskii, N.A. Pikhtin, A.Y. Egorov. Techn. Phys. Lett., **45** (4), 398 (2019).
[15] A.V. Babichev, D.A. Pashnev, A.G. Gladyshev, A.S. Kurochkin, E.S. Kolodeznyi, L.Y. Karachinsky, A.Y. Egorov. Opt. Spectrosc., **128** (8), 1187 (2020).
[16] A.J. Ward, D.J. Robbins, D.C.J. Reid, N.D. Whitbread, G. Busico, P.J. Williams, J.P. Duck, D. Childs, A.C. Carter. IEEE Phot. Techn. Lett., **16** (11), 2427 (2004).
[17] A. Sadeghi, P.Q. Liu, X. Wang, J. Fan, M. Troccoli, C.F. Gmachl. Opt. Express, **21** (25), 31012 (2013).
[18] A.V. Babichev, D.A. Pashnev, A.G. Gladyshev, D.V. Denisov, G.V. Voznyuk, L.Y. Karachinsky, I.I. Novikov, M.I. Mitrofanov, V.P. Evtikhiev, D.A. Firsov, L.E. Vorob'ev, N.A. Pikhtin, A.Y. Egorov. Techn. Phys. Lett., **46** (4), 312 (2020).
[19] B.G. Lee, M.A. Belkin, R. Audet, J. MacArthur, L. Diehl, C. Pflügl, F. Capasso, D.C. Oakley, D. Chapman, A. Napoleone, D. Bour, S. Corzine, G. Höfler, J. Faist. Appl. Phys. Lett., **91** (23), 231101 (2007).
[20] P. Jouy, C. Bonzon, J. Wolf, E. Gini, M. Beck, J. Faist. Appl. Phys. Lett., **106** (7), 071104 (2015).
[21] C. Boyle, C. Sigler, J.D. Kirch, D.F. Lindberg, T. Earles, D. Botez, L.J. Mawst. Appl. Phys. Lett., **108** (12), 121107 (2016).
[22] A.Y. Egorov, A.V. Babichev, L.Y. Karachinsky, I.I. Novikov, E.V. Nikitina, M. Tchernycheva, A.N. Sofronov, D.A. Firsov, L.E. Vorobjev, N.A. Pikhtin, I.S. Tarasov. Semiconductors, **49** (11), 1527 (2015).
[23] A.V. Babichev, E.S. Kolodezny, A.G. Gladyshev, D.V. Denisov, G.V. Voznyuk, M.I. Mitrofanov, N.Yu. Kharin, V.Yu. Panevin, S.O. Slipchenko, A.V. Lyutetsky, V.P. Yevtikhiev, L.Ya. Karachinsky, I.I. Novikov, N.A. Pikhtin, A.Yu. Yegorov. FTP, **55** (7), 602 (2021) (in Russian).
[24] M. Razeghi, W. Zhou, S. Slivken, Q.Y. Lu, D. Wu, R. McClintock. Appl. Optics, **56** (31), H30 (2017).
[25] H. Kogelnik, C.V. Shank. J. Appl. Phys., **43** (5), 2327 (1972).
[26] M. Brandstetter, A. Genner, C. Schwarzer, E. Mujagic, G. Strasser, B. Lendl. Opt. Express, **22** (3), 2656 (2014).
[27] H. Knötig, B. Hinkov, R. Weih, S. Höfling, J. Koeth, G. Strasser. Appl. Phys. Lett., **116** (13), 131101 (2020).
[28] M. Holzbauer, R. Szedlak, H. Detz, R. Weih, S. Höfling, W. Schrenk, J. Koeth, G. Strasser. Appl. Phys. Lett., **111** (17), 171101 (2017).

[29] C. Schwarzer, E. Mujagić, S.I. Ahn, A.M. Andrews, W. Schrenk, W. Charles, C. Gmachl, G. Strasser. Appl. Phys. Lett., **100** (19), 191103 (2012).
[30] E. Mujagić, M. Nobile, H. Detz, W. Schrenk, J. Chen, C. Gmachl, G. Strasser. Appl. Phys. Lett., **96** (3), 031111 (2010).
[31] A.V. Babichev, E.S. Kolodeznyi, A.G. Gladyshev, D.V. Denisov, N.Yu. Kharin, A.D. Petruk, V.Yu. Panevin, S.O. Slipchenko, A.V. Lyutetskii, L.Ya. Karachinsky, I.I. Novikov, N.A. Pikhtin, A.Yu. Egorov. Tech. Phys. Lett., **48** (3), 6 (2022).
[32] C. Schwarzer, R. Szedlak, L. Burgstaller, A. Genner, T. Zederbauer, H. Detz, A.M. Andrews, W. Schrenk, G. Strasser. *Proc. 2013 Conf. on Lasers and Electro-Optics — Int. Quantum Electronics Conf.* (Munich, Germany, Optica Publishing Group, 2013), paper CB_2_3.
[33] R. Szedlak, M. Holzbauer, D. MacFarland, T. Zederbauer, H. Detz, A.M. Andrews, C. Schwarzer, W. Schrenk, G. Strasser. Sci. Rep., **5**, 16668 (2015).
[34] E. Mujagić, L.K. Hoffmann, S. Schartner, M. Nobile, H. Detz, D. Andrijasevic, M. Austerer, W. Schrenk, A.M. Andrews, P. Klang, M.P. Semtsiv, W.T. Masselink, G. Strasser. Proc. SPIE, **7230**, 723015 (2009).